Received 7 December 2023; revised 16 January 2024; accepted 5 February 2024. Date of publication 12 February 2024; date of current version 6 August 2024.

Digital Object Identifier 10.1109/OJAP.2024.3365039

2-D Ray-Tracing Model for Multilayer Dielectric Dome Arrays With Inner Reflections

MARIA PUBILL-FONT[1], FRANCISCO MESA[2] (Fellow, IEEE), ASTRID ALGABA-BRAZÁLEZ[3], SARAH CLENDINNING[4], MARTIN JOHANSSON[3] (Senior Member, IEEE), AND OSCAR QUEVEDO-TERUEL[4] (Fellow, IEEE)

[1]The Global Big Data Technologies Center, University of Technology Sydney, Ultimo, NSW 2007, Australia
[2]Department of Applied Physics 1, Universidad de Sevilla, 41012 Sevilla, Spain
[3]Ericsson Research, Ericsson AB, 417 56 Gothenburg, Sweden
[4]Division of Electromagnetic Engineering and Fusion Science, KTH Royal Institute of Technology, 100 44 Stockholm, Sweden

CORRESPONDING AUTHOR: O. QUEVEDO-TERUEL (e-mail: oscarqt@kth.se)

The work of Francisco Mesa was supported in part by MCIN/AEI/10.13039/501100011033 under Grant PID2020-116739GB-I00. The work of Astrid Algaba-Brazález, Martin Johansson, and Oscar Quevedo-Teruel was supported by the Strategic Innovation Program Smarter Electronics System—a Joint Venture of Vinnova, Formas, and the Swedish Energy Agency under Project 2023-00648.

ABSTRACT The application of lenses combined with array antennas (also known as dome arrays or dome antennas) to the next generation of terrestrial and satellite communication systems brings a wide range of advantages in terms of improved radiation performance, reconfigurability in the use case, and reduction in power consumption. To facilitate the industrial implementation of dome antennas, highly efficient simulation tools are required. In this paper, we present a streamlined implementation of ray tracing for fast and efficient numerical analysis of the far-field radiation performance of 2D multilayer dielectric lenses combined with phased arrays. Unlike commercial physical-optical methods, our proposed ray-tracing method is capable of computing the effects of internal reflections in the dome in a multilayer configuration. In addition, the method estimates the absorption losses as a result of the Joule effect. To demonstrate the effectiveness of the proposed approach, we provide comparisons of the simulated radiation patterns using our proposed ray tracing with the results obtained from commercial full-wave simulation tools.

INDEX TERMS Array antenna, absorption loss, dielectric lens, dome, matching layers, lens array, ray tracing, radiation pattern, reflection losses, scanning, 6G.

I. INTRODUCTION

THE INTRODUCTION of the sixth generation (6G) [1] mobile communications is anticipated for 2030, and it is expected to have a much greater effect on our society than 5G. Examples of 6G use cases include sensorial experiences (Internet of Senses), machine-type communication, augmented reality and virtual reality (AR/VR), and joint communication and sensing (JCAS). To meet the needs of an increasing number of connected devices and users, 6G must allocate additional spectrum that has not been used before, as well as address critical technological issues related to hardware and antenna solutions [2].

Phased array antennas (PAA) constitute an interesting antenna solution for 5G/6G terrestrial communications [3], [4], [5] and satellite systems [6] due to their simplicity of design and beam steering capability, which can be achieved without physically moving the antenna. However, the performance of electronically scanned PAA is compromised when steering toward extreme angles due to a reduction in the projected antenna aperture size in the scanning direction, resulting in increased scanning losses [7], [8]. Antennas capable of achieving wide beam scanning without performance degradation are highly desirable for some applications, such as radars systems [9], aircraft-satellite communications systems [10], [11], and modern wireless communication systems [12], [13]. An attractive solution is the combination of phased arrays with quasi-optical systems, which provides good matching performance and

high gain for large scanning angles. Well-known solutions include pillbox antennas [14], [15], [16], Rotman lenses [17], [18], [19], Luneburg lenses (which can be implemented in a fully metallic form with metasurfaces [20] or geodesic surfaces [21]), shaped parallel plate lenses [22], and homogeneous dielectric lenses [23], [24], [25], [26], [27].

The combination of dielectric lenses and arrays, known as dielectric dome antennas, is a promising antenna solution for the next generation of radio access systems and satellite communications [27], [28], [29], [30], [31], [32], [33]. These antennas can be used to enhance certain properties of phased arrays, such as their field of view [7], [26], to modify their radiating performance to suit different scenarios[34], or to reduce the power consumption of power amplifiers to achieve a specific Equivalent Isotropic Radiated Power (EIRP) value [35]. When the goal is to increase the operating scanning range, the dome introduces the phase variation required to deflect the beam in the desired direction [36], and due to the vertical dimension of the lens, the effective aperture will increase. A dome antenna could be implemented with metasurfaces [37], but this would lead to a narrow operating bandwidth caused by the narrowband behavior of the employed metasurface. The most practical approach is the dome implementation based on homogeneous dielectrics, because of its simplicity of design and cost-effectiveness. Furthermore, by choosing the lens material in a suitable way, the dome may also act as a radome. In this way, we add lensing functionality to the radome, which allows us to improve the scanning performance of the array while providing mechanical protection from the environment. The lens curvature is then selected to manipulate the wavefront and obtain the desired focusing properties for each specific application. Therefore, the shape of the dome could be optimized by modifying its geometry for different use cases according to the required specifications, as previously introduced in [34]. Additional dielectric layers, known as matching layers, can be introduced to reduce the number of reflections occurring at the air/dome boundaries.

The optimization of lens/radome shapes using commercial full-wave simulators is computationally intensive and time-consuming. To address this issue, ray-tracing techniques have been developed to evaluate the far-field performance of large objects with reduced time and computational resources [38], [39], [40], [41], [42], [43], [44], [45], [46], [47], [48], [49], [50], [51]. Additionally, there are commercial software packages available for this purpose [52], [53]. Recently, a numerical method based on ray tracing to evaluate the far field of generalized geodesic lenses was proposed in [54].

Although the general area of ray-tracing techniques can be considered mature (mainly due to its extensive use in computer graphic tools), the opportunity for advancement still remains in specific cases; for example, in the study of dome antennas, where simplifications can be made to significantly reduce simulation time. If we are only interested in ray-tracing for a particular purpose rather than using a generalized commercial ray-tracing software, there are a number of open source libraries available (e.g., [55], [56], [57]), as well as the ray-tracing tool specifically proposed in [7], to evaluate the effect of homogeneous dielectric lenses in dome antennas without considering reflection or absorption losses. This paper presents an extended but still simplified and efficient ray-tracing tool to evaluate the radiation characteristics of two-dimensional (2D) multilayer dielectric dome antennas, taking into account reflection and absorption losses. The simplified 2D model also allows us to investigate the effect of matching layers to mitigate reflection losses. As previously mentioned in [32], 2D models can give us a good understanding of the performance of a three-dimensional (3D) dome array antenna. In contrast to [32], the H-plane radiation pattern of the dome array is computed here using the straightforward Kirchhoff diffraction formula that was already used in [54]. The numerical effectiveness and accuracy of the radiation patterns computed with the reported simplified method have been demonstrated and compared with the COMSOL Multiphysics software for the 2D case and with the CST Microwave Studio for the 3D case. This tool can be used as a primary step for the design of 3D lenses and domes for 5G/6G communication, as it provides a good initial qualitative and quantitative insight into the lens performance. The proposed method is especially advantageous when different dome structures are needed to adjust the radiating performance of an array antenna to different use cases, as described in [34], thus meeting the customer's requirements in a timely manner, since the array can be reused and only the dome design needs to be modified.

II. RAY-TRACING MODEL

In this section, we discuss several aspects of the numerical implementation of the simplified ray-tracing technique proposed to analyze dielectric dome antennas. Rather than using some of the more comprehensive and rigorous asymptotic methods already reported in the literature [27], [39], [42], [43], [46], [51], the straightforward implemented method has been inspired by the one reported in [54], although it has been adapted to handle multilayer dielectric 2D lenses combined with an array. The ray-tracing approach is based on three underlying theories: 1) geometrical optics (GO), used to determine the trajectories of the rays, 2) conservation of ray tube power, applied to calculate the amplitude distribution at the lens aperture, and 3) the Kirchhoff diffraction formula, employed to obtain the far-field pattern.

To test our ray-tracing approach, we used a dome reference model from [7]. The geometry of the dome is shown in Fig. 1, and is characterized by its dielectric constant, ε_r, with inner and outer surfaces s_1 and s_2. The surfaces are rotationally symmetric with respect to the vertical z axis and follow conic shapes. In this work, the dielectric dome of $\varepsilon_r = 2.5$ is evaluated with an array of $L = 975$ mm at 13 GHz.

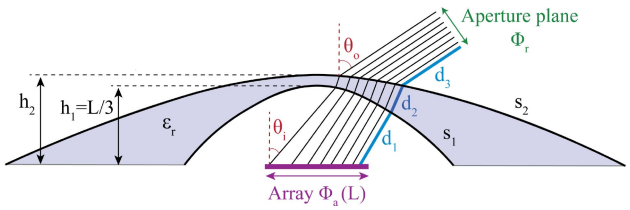

FIGURE 1. Dielectric dome antenna geometry and main parameters.

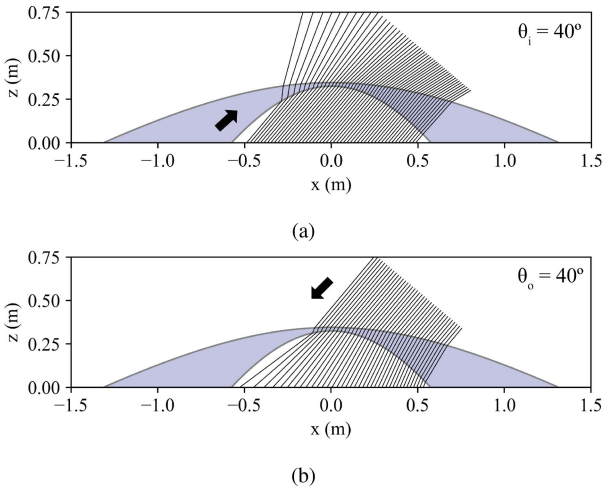

FIGURE 2. Examples of (a) *direct ray tracing* for linear phase array excitation and (b) *reverse ray tracing* for calculating the phase over the array.

A. GEOMETRICAL OPTICS

GO uses a zero-wavelength approximation to model the behavior of electromagnetic propagation in terms of rays [58], [59]. The rays are defined as the orthogonal trajectories to the wavefronts, which are the equiphase surfaces of a wave. To trace the rays through dielectric lenses, the Snell-Descartes law is employed. Following the procedure reported in [7], two different approaches to ray tracing are presented here, depending on where the starting points of the rays are set. The first, referred to as *direct ray tracing*, involves setting the starting points in the array. This ray tracing is the initial step in obtaining the amplitude distribution and the far-field radiation pattern. The second implementation is *reverse ray tracing*, in which the starting points are specified in the aperture plane. Reverse ray tracing is used to obtain the optimum phase distribution over the array to maximize directivity. For completeness, this procedure is briefly outlined next.

1) DIRECT RAY TRACING

The rays are emitted from the array towards the aperture plane, with a fixed angle of emergence, θ_i, as seen in Fig. 2(a). This initial step considers the case of a linear phased array excitation, meaning that all the rays have the same incident angle, θ_i, and are parallel to each other at the source. However, since the surfaces of the dome are not parallel, the rays will be deflected in different directions, leading to a decrease in directivity. Consequently, an optimal phase distribution is needed to maximize performance.

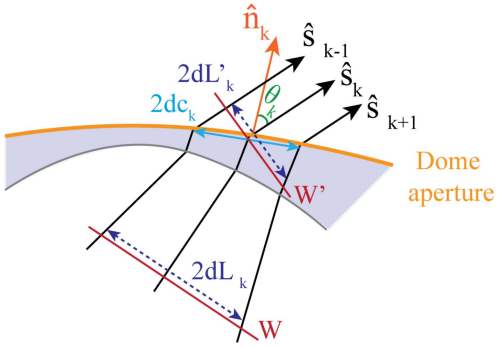

FIGURE 3. Schematic of the *k*-th ray tube and variables involved in the amplitude evaluation.

2) REVERSE RAY TRACING

Rays are sent out from the aperture plane towards the array in order to maximize directivity. We assumed that the rays in the outer part of the dome are parallel, so they reach the surface where the array is located (at $z = 0$) with a nonlinear phase distribution. The angle at which the rays impinge on the dome [θ_o in Fig. 2(b)] is the same for all rays. The phase distribution is obtained by adding the effective distances traveled inside the different media for each ray [7]:

$$\Phi_a = -(d_1 k_0 + d_2 k_d + d_3 k_0) \tag{1}$$

where the distances $d_{1,2,3}$ are shown in Fig. 1 for a specific ray, and k_0 and $k_d = k_0\sqrt{\varepsilon_r}$ are the wavenumbers in free space and in the lens material, respectively.

B. RAY TUBE POWER THEORY

Since the rays are not parallel, the power distribution at the aperture is different from that at the source. Conservation of power within the ray tubes is applied to account for this effect [58]. Some details on the calculation of the amplitude at the lens aperture were previously given in [54]. Following the notation in Fig. 3, the amplitude can be expressed as

$$A'_k = A_k \sqrt{\frac{\mathrm{d}L_k}{\mathrm{d}c_k \cos\theta_k}} \tag{2}$$

where A'_k is the electric field amplitude of the ray k on the dome aperture wavefront, W'. The terms A_k and $\mathrm{d}L_k$ refer to the amplitude and width of the ray tube on the source wavefront, defined as W. The term $\mathrm{d}c_k$ refers to the length of the arc in the dome aperture, and we define θ_k as the angle between the local normal unit vector to the aperture $\hat{\mathbf{n}}_k$ and the local Poynting unit vector $\hat{\mathbf{s}}_k$. All the parameters needed for the amplitude calculation are obtained from the GO. Since the wavefront W' and the dome aperture can have different curvatures, the width of the ray tube in the dome aperture, $\mathrm{d}L'_k$, is taken as $\mathrm{d}c_k \cos\theta_k$.

C. RADIATION PATTERN COMPUTATION

The far-field radiation pattern is evaluated using the Kirchhoff diffraction formula [54], given by

$$E(\theta) \propto \sum_k A'_k \frac{\mathrm{e}^{-\mathrm{j}k_0(r_k+\sigma_k)}}{r_k} \left[\hat{\mathbf{n}}_k \cdot \hat{\mathbf{s}}_k + \hat{\mathbf{n}}_k \cdot \hat{\mathbf{r}}_k\right] T_k \, \mathrm{d}c_k \quad (3)$$

where $E(\theta)$ is the total far-zone electric field at a given observation angle θ. The dome aperture is treated as an array of radiating dipoles, each with an amplitude A'_k. σ_k is the effective path length of the k-th ray from the source to the lens aperture (this quantity is defined later), r_k is the distance from the aperture to the observer position, $\hat{\mathbf{r}}_k$ is the unit vector in the direction of the dome aperture to the observer point. The term T_k is the Fresnel transmission coefficient [60] that accounts for all reflections.

III. STUDY OF LOSSES

In dielectric dome antennas, absorption and reflection can lead to losses. We have modified the ray-tracing approach from [54] to evaluate these phenomena. Our approach enables us to incorporate a dielectric material with a given loss tangent and calculate the associated material losses. Additionally, the forward and backward fields propagating across different interfaces are related to the transfer matrix. We use the matrix solution to calculate the components of transmitted and reflected electromagnetic waves for a multilayer dielectric structure in order to evaluate reflection losses [60], [61].

A. ABSORPTION LOSSES

The dielectric loss tangent, $\tan\delta$, is a measure of the electrical energy dissipated due to various physical processes, such as dielectric relaxation, dielectric resonance, electrical conduction, and nonlinear losses [62]. When the medium is not ideal, absorption losses must be taken into account, and the dielectric constant of the material becomes complex, $\varepsilon = \varepsilon' - \mathrm{j}\varepsilon''$. Then, the wavenumber $k = \beta - \mathrm{j}\alpha$ (β and α are the phase and attenuation constants) associated with a homogeneous medium can be written as

$$k = \omega\sqrt{\mu_0\varepsilon'(1 - \mathrm{j}\tan\delta)} = k_0\sqrt{\varepsilon_\mathrm{r}(1 - \mathrm{j}\tan\delta)} \quad (4)$$

with ε_r being the relative permittivity constant of the medium, and $\tan\delta$ the ratio between the real and imaginary parts of ε (isotropic magnetic lossless/lossy materials can easily be taken into account by changing μ_0 by its corresponding magnetic permeability). The complex permittivity of each material in a layered dielectric dome leads to different wavenumbers. This is taken into account when the far field is evaluated using the Kirchhoff diffraction formula (3). The total effective path of the k-th ray, which can be complex if $\tan\delta_i \neq 0$, is then given by the effective path length

$$\sigma_k = \sum_{i=1}^{N} \sigma_k^{(i)} = \sum_{i=1}^{N} \sqrt{\varepsilon_{\mathrm{r},i}(1 - \mathrm{j}\tan\delta_i)}\,\Delta_i \quad (5)$$

where the index i represents each medium of the N-layered structure and Δ_i is the geometric distance traveled by the ray within the i-th material.

B. REFLECTION LOSSES

When a traveling plane wave impinges on an interface between two materials with different permittivities, both reflection and refraction occur. However, when the medium is layered, it is not enough to calculate the reflections at each interface, as some of the energy will be trapped inside one material as a result of internal reflections. According to [61], [63], [64], the reflection and transmission losses associated with each ray in a planar layered medium can be determined by using propagation/matching matrices for transverse fields. The losses due to multiple reflections can then be calculated using the complex transmission coefficient T_k in the Kirchhoff diffraction formula (3).

The analysis of transmission and reflection coefficients for a multilayer planar dielectric medium can be accomplished using the following approach outlined in [61], [63], [64]:

$$\begin{bmatrix} E_0^+ \\ E_0^- \end{bmatrix} = \left\{ \prod_{i=1}^{N+1} \frac{1}{T_i} \begin{bmatrix} \mathrm{e}^{\mathrm{j}\varphi_i} & R_i\mathrm{e}^{-\mathrm{j}\varphi_i} \\ R_i\mathrm{e}^{\mathrm{j}\varphi_i} & \mathrm{e}^{-\mathrm{j}\varphi_i} \end{bmatrix} \right\} \begin{bmatrix} E_{N+1}^+ \\ 0 \end{bmatrix} = \begin{bmatrix} A_{11} & A_{12} \\ A_{21} & A_{22} \end{bmatrix} \begin{bmatrix} E_{N+1}^+ \\ 0 \end{bmatrix} \quad (6)$$

where T_i and R_i are the Fresnel transmission and reflection coefficients, respectively, at the i-th interface between the $(i-1)$-th and i-th layers. The phase shift associated with each layer is given by $\varphi_i = k_i \cos\theta_i t_i$, where t_i is the thickness of the layer and θ_i is the propagation angle with respect to the normal of the interface ($\varphi_{N+1} = 0$). The total transmission coefficient for each ray is obtained after computing the product of the matrices as $T_k = 1/A_{11}$. The above derivation assumes that all interfaces are planar and parallel, so (6) must be adapted for our case study, where the surfaces of the dielectric dome have a conical shape. To do this, the geometry of the problem can be simplified by breaking down all the surfaces that make up the dome into small segments/facets.

The matrix solution requires three inputs: the thickness of each layer, the relative permittivity of each layer, and the angle of incidence. The configuration in Fig. 4(a) is used as an approximate equivalent local model of the layered lens when the surfaces are not parallel, for the particular case of a three-layer dielectric slab. The normal of the first surface, $\hat{\mathbf{n}}_A$, is traced at the intersection point of the incoming ray with this surface, a point that will be used as a reference. Each time the ray intersects another interface, an auxiliary line parallel to the first surface is traced [blue dashed lines in Fig. 4(a)]. The "effective" thickness of each layer, t'_i, is taken as the distance between the parallel auxiliary lines, thus creating a locally effective planar structure, acceptable for the evaluation of the reflection losses associated with each individual ray. The use of this equivalent planar model to calculate the transmission coefficient T_t ignores any phase

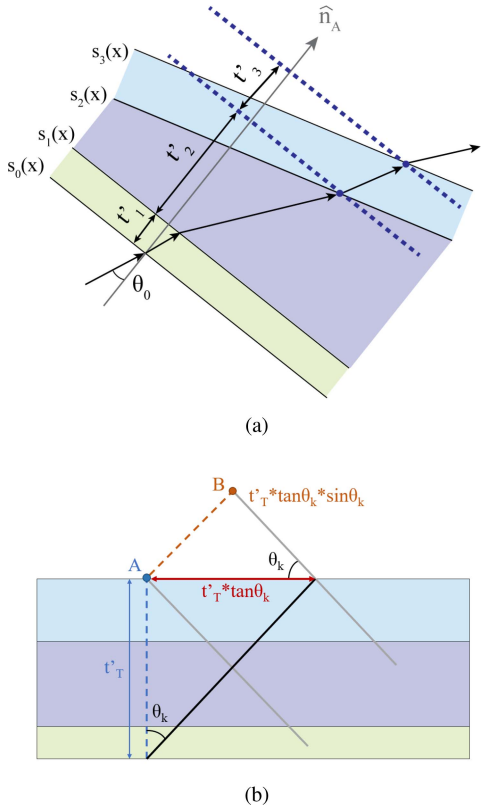

FIGURE 4. (a) Original locally non-planar structure and the equivalent thickness used to evaluate reflections in the discretized dome. (b) Effective locally-planar model that shows the phase compensation for the plane wave model.

shift of the ray due to its original non-planar nature. However, in our approximate model, we must take into account a phase-shift factor ξ_k for each ray. This requires moving the reference from point A to the corresponding exit point of the ray, point B in Fig. 4(b), which makes that

$$\xi_k = \mathrm{e}^{-\mathrm{j}k_0 t'_T \tan\theta_k \sin\theta_k} \tag{7}$$

where the angle θ_k between the ray inside the lens and the normal $\hat{\mathbf{n}}_A$ is determined by the Snell-Descartes law, which states that $\theta_k = \arcsin(\sin\theta_0/n_{\text{lens}})$. The total equivalent thickness t'_T in the case of Fig. 4 is equal to the sum of t'_1, t'_2, and t'_3. The distance from the end-point of the ray to point A (solid red line in Fig. 4) is obtained from $t'_T \tan\theta_k$. Then the term $\sin\theta_k$ is added to the phase-shift factor ξ_k to move the reference from point A to point B (dashed orange line). The accuracy of the approximate equivalent local planar model is demonstrated by the close match between the results of our model and full-wave simulations, which is discussed in more detail in the following sections.

IV. NUMERICAL RESULTS

The 2D dielectric dome array antenna was modeled using the ray-tracing tool discussed in the previous section. The dome shapes were divided into 30 segments, which was enough to guarantee good convergence in this case. To validate the precision and efficiency of our approach, we also simulated

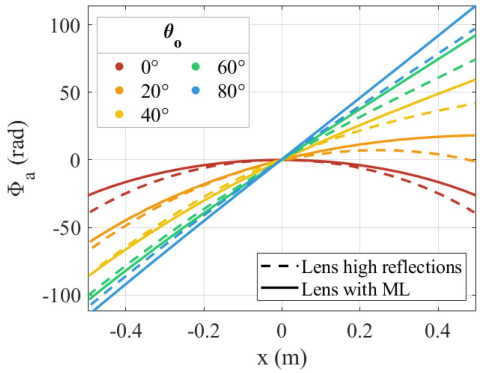

FIGURE 5. Phase distributions in the array when a plane wave is arriving from θ_o of 0°, 20°, 40°, 60° and 80°.

the 2D profile of the lens with COMSOL at 13 GHz. The dielectric lens was illuminated using an 84-element array of dipoles with a length of 975 mm (see Fig. 1). Two lenses were simulated: a three-layer dome with arbitrary refractive indexes and high reflection losses and a dielectric dome with matching layers. The reverse ray tracing is used to obtain the phase excitation of the array when the lens is applied. The phases are shown in Fig. 5 for the two lenses studied: the lens with high reflections and the lens with matching layers. However, the radiation patterns are computed with direct ray tracing using the phase information obtained from the reverse model (from Fig. 5).

A. DOME WITH HIGH REFLECTIONS

A conic-shaped dome with three layers of different refractive indices is used to test the accuracy of the proposed ray-tracing tool in assessing reflection losses. The refractive indices of the layers are 3, 4, and 2.5, respectively, and the 2D profile is shown in Figure 6(a). The thicknesses of the first and third layers are $t_1 = 20$ mm and $t_3 = 30$ mm. The shape of the lens is defined by four surfaces (s_0, s_1, s_2, and s_3) that can be defined analytically or numerically, resulting in four functions that are discretized. In this example, the surfaces s_0 and s_1 that define the lower dielectric layer have the same shape; similarly, s_2 and s_3 that bound the upper layer are also parallel to each other. When the surfaces are discretized, the problem can be locally viewed as two nonparallel but planar surfaces, s_1 and s_2, with additional parallel lower and upper parallel surfaces, s_0 and s_3, as illustrated in Fig. 4(a).

Fig. 6(b) shows the radiation patterns for 0°, 20°, 40°, 60° and 80°, comparing the results obtained with our algorithm and the COMSOL software. The phase distribution of the phased array is obtained first from reverse ray tracing, as discussed in Section II-A. The peak magnitude of the electric field normalized to that in broadside without the lens is illustrated in Fig. 6(c). The ray-tracing results are compared to those from COMSOL simulations, as well as to the scan losses of the isolated array (gray line). The comparison yields good agreement across the entire scanning range, although some minor discrepancies are observed for large angles,

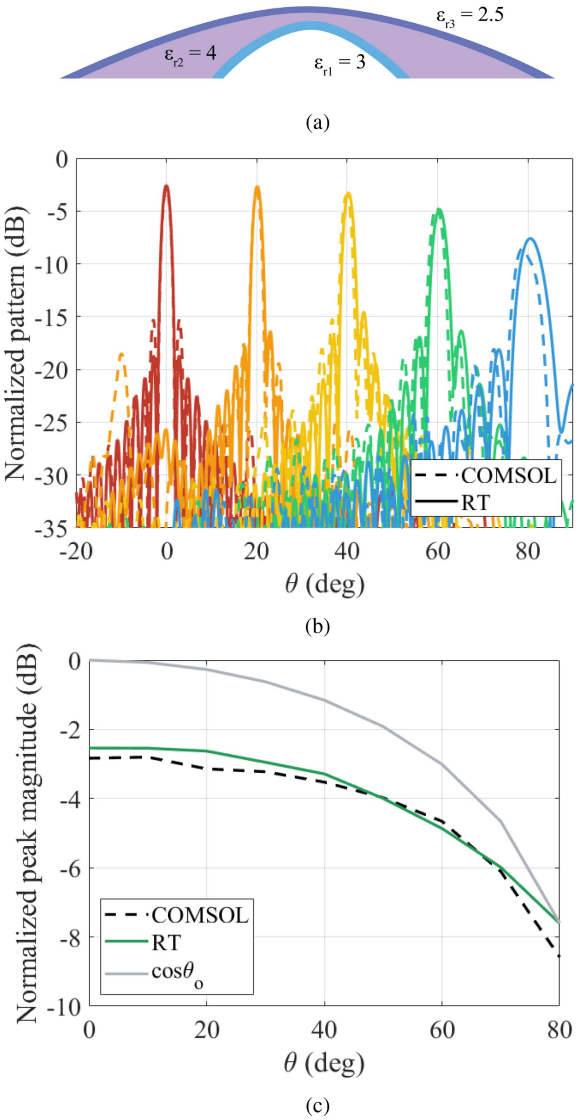

FIGURE 6. (a) 2D profile, (b) radiation patterns, and (c) peak magnitude vs scanning angle for a conic-shaped dielectric lens with high reflections. Ray-tracing results are compared with COMSOL.

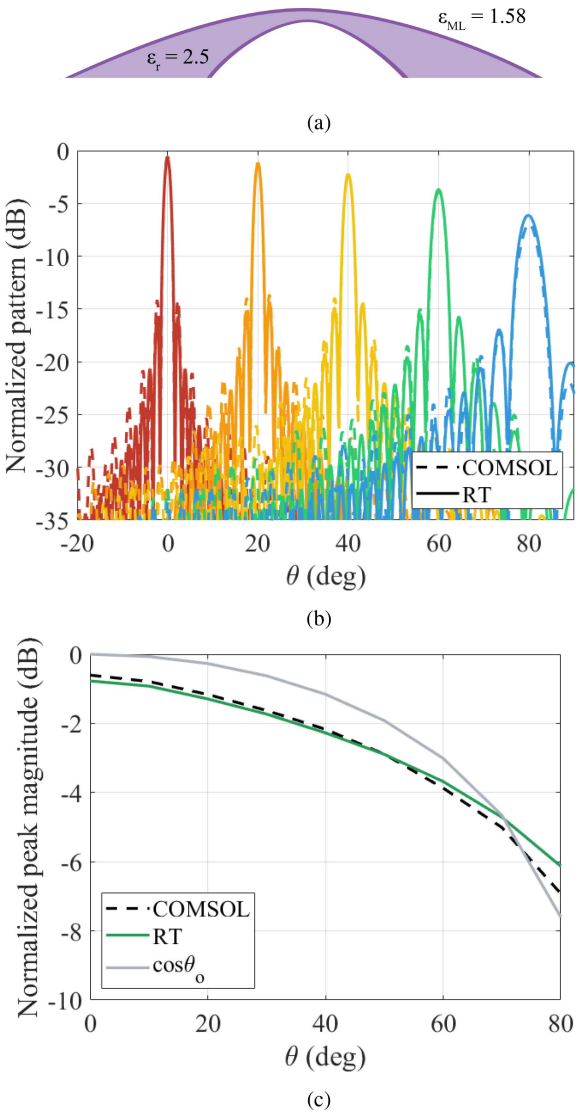

FIGURE 7. (a) 2D profile, (b) radiation patterns, and (c) peak magnitude vs scanning angle for a conic-shaped dielectric lens with matching layers. Ray-tracing results are compared with COMSOL.

which are mainly attributed to the drawbacks of COMSOL when simulating such extreme angles. A simulation of the isolated array without the lens was also conducted using COMSOL and was compared to the ray-tracing algorithm, which revealed similar discrepancies at these large angles.

B. DOME WITH MATCHING LAYERS

Here we study a dielectric dome of $\varepsilon_r = 2.5$ defined by two surfaces s_1 and s_2 when this dome is bounded by lower and upper matching layers. To reduce the level of reflections, these matching layers have a thickness of a quarter wavelength and a relative permittivity $\varepsilon_{ML} = \sqrt{1 \cdot 2.5} = 1.58$. The shapes of the four surfaces that define this lens are exactly the same as in the previous example, as shown in Fig. 7(a).

In Fig. 7(b), the radiation patterns computed with COMSOL and the ray-tracing algorithm are presented with the phase distribution of the phased array obtained first from reverse ray tracing. Radiation patterns are computed for five cases, each with a different pointing direction that goes from 0° to 80°. The peak magnitude of the electric field normalized to that in broadside without the lens is illustrated in Fig. 7(c). Again, good agreement is achieved along almost the entire scanning range between the ray-tracing (RT) and COMSOL data. Similarly to the previous example, small discrepancies are found for very large pointing angles. This analysis clearly shows that matching layers are required to reduce losses.

Our model has also been tested using CST Studio Suite 2022, a three-dimensional (3D) full-wave simulator. Two lenses were implemented in CST at 28 GHz and

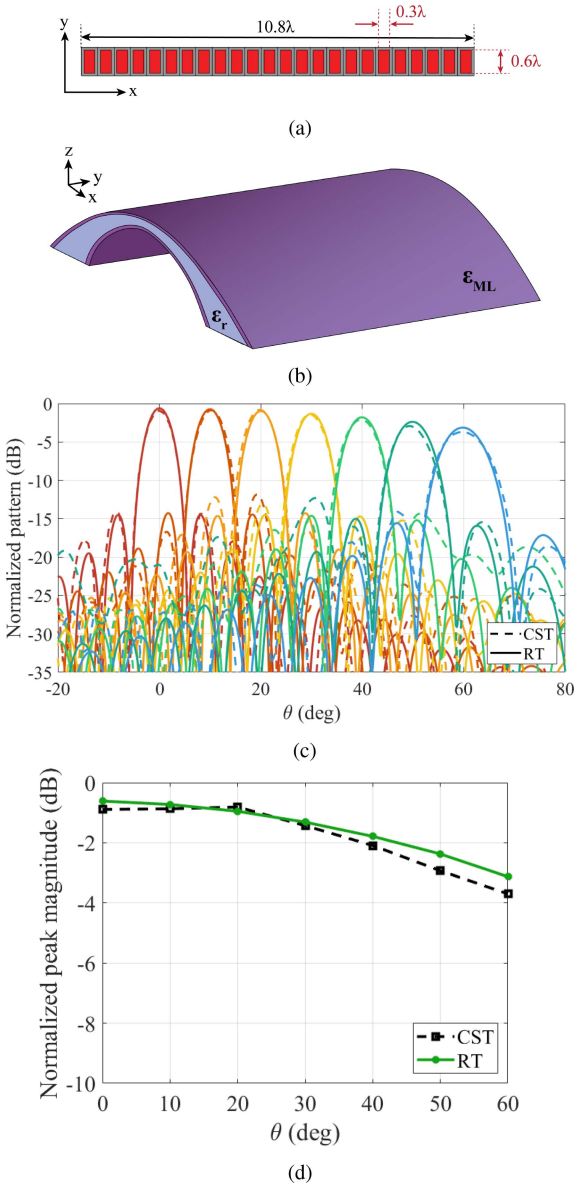

FIGURE 8. (a) Linear phased array,(b) cylindrical lens, (c) radiation patterns considering CST and 2D ray-tracing, and (d) peak magnitude vs scanning angle for conic-shaped dielectric lens with matching layers. The results are normalized to broadside without the lens.

compared to the proposed ray-tracing tool. Figure 8(a) shows a one-dimensional array of 24 waveguides that illuminates a cylindrical lens along the y-axis. The dimensions of the array and the 2D profile of the lens were taken from [34]. The geometry of the 3D lens is depicted in Fig. 8(b), and the radiation patterns for different steering directions in the E-plane are shown in Fig. 8(c). To assess the effect of reflection losses, the results were normalized to the broadside without the lens. For the second validation, a two-dimensional array of 24x8 waveguides was employed, as depicted in Fig. 9(a). The second lens had the same profile as the first, but was rotationally symmetric with respect to the z-axis, as illustrated in Fig. 9(b). The radiation patterns

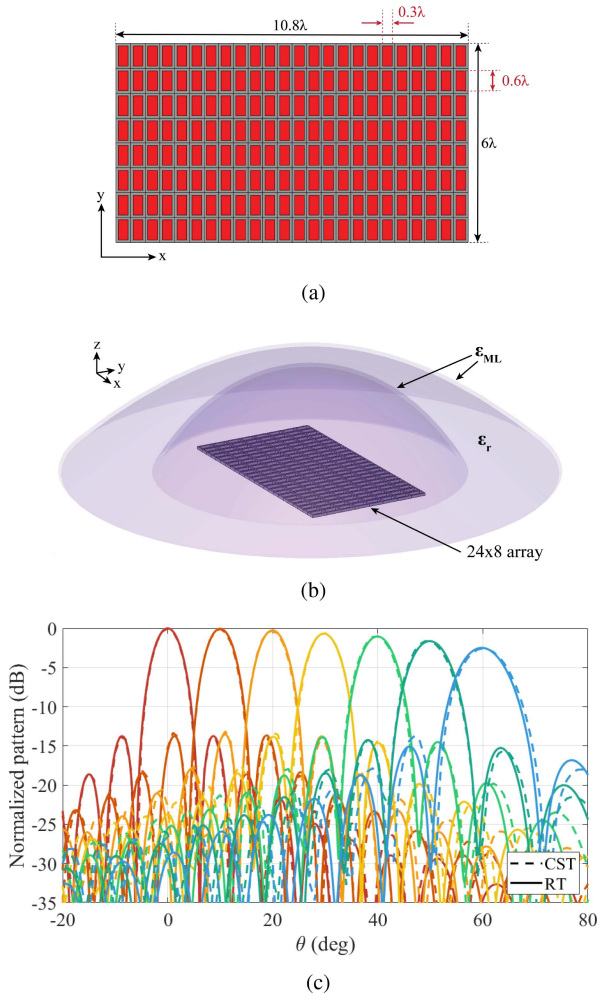

FIGURE 9. (a) 2D Phased array model included in the CST simulation. (b) Spherical lens, (c) radiation patterns normalized to broadside with the lens for a rotationally symmetric conic-shaped dielectric lens.

of the lens normalized to broadside are shown in Fig. 9(c). The radiation patterns show the E_x-field contribution in the E-plane, which corresponds to the co-polarization. In this simulation, although it is not illustrated here, the cross-polarization is negligible. The results obtained from the 2D ray-tracing model and the CST tool for both the cylindrical and spherical lenses were in very good agreement. This shows that the proposed method can be used as a first design step for 3D dome antennas, as it provides a reliable initial understanding of the lens performance, both qualitatively and quantitatively.

As a final note, the CPU time employed by the ray-tracing tool implemented in these two examples is about 150 times less than that required by COMSOL, 240 times less than the required in CST for the cylindrical lens, and 740 times less for the spherical lens in CST.

V. CONCLUSION

An efficient ray-tracing tool has been developed to evaluate the far-field radiation pattern of 2D multilayer dielectric lenses. Radiated fields computed with this approach

have been successfully validated by comparison with the COMSOL commercial simulator, reducing the computational time by a factor of approximately 150. Losses can be determined even when extra layers are added to the dielectric dome. The imaginary part of the permittivity of the layers is used to take into account absorption losses. Reflection losses have been accurately simulated by utilizing an equivalent local planar model and the propagation/matching matrices for the transverse fields. The implementation of the ray-tracing method has been proven to be a powerful and precise tool for the design and analysis of multilayer dielectric dome antennas. The 2D ray-tracing model has also been verified with a 3D full-wave commercial simulator, CST Studio Suite 2022, demonstrating its suitability as an initial design tool for understanding how a 3D lens shape would perform when combined with an array. This has a significant industrial impact, as different lens geometries can be modeled quickly and accurately, saving computational resources and engineering efforts. The agreement between our simplified 2D model and CST is remarkable. However, to make the ray-tracing approach suitable for all dome antenna applications, our next research objective is to expand the ray-tracing method to encompass 3D structures. Moreover, the proposed methodology has shown significant efficiency and speed, making it a valuable complement to advanced synthesis procedures. Exploring synthesis methods for dome antenna design will be considered for future research.

ACKNOWLEDGMENT

The authors would like to thank Lic. Eng. Pilar Castillo-Tapia from KTH Royal Institute of Technology, and Lic. Eng. Lars Manholm from Ericsson Research, for the support on the supervision of this project and the fruitful technical discussions.

REFERENCES

[1] G. Wikström et al., (Ericsson, Stockholm, Sweden). *6G–Connecting a Cyber-Physical World*. Feb. 2022. [Online]. Available: https://www.ericsson.com/en/reports-and-papers/white-papers/a-research-outlook-towards-6g

[2] I. Andersson, L. Manholm, A. Algaba-Brazález, and P. Aghdam, "Antenna system requirements and challenges towards 6G–an industrial view," in *Proc. Int. Workshop Antenna Technol. (iWAT)*, 2023, pp. 1–4.

[3] A. Osseiran et al., (Ericsson, Stockholm, Sweden). *5G Wireless Access: An Overview*. Apr. 2020. [Online]. Available: https://www.ericsson.com/en/reports-and-papers/white-papers/5g-wireless-access-an-overview

[4] K. Kibaroglu, M. Sayginer, T. Phelps, and G. M. Rebeiz, "A 64-element 28-G Hz phased-array transceiver with 52-dBm EIRP and 8–12-Gb/s 5G link at 300 meters without any calibration," *IEEE Trans. Microw. Theory Techn.*, vol. 66, no. 12, pp. 5796–5811, Dec. 2018.

[5] M. Li, S.-L. Chen, Y. Liu, and Y. J. Guo, "Wide-angle beam scanning phased array antennas: A review," *IEEE Open J. Antennas Propagat.*, vol. 4, pp. 695–712, 2023.

[6] T. Chaloun et al., "Electronically steerable antennas for future heterogeneous communication networks: Review and perspectives," *IEEE J. Microw.*, vol. 2, no. 4, pp. 545–581, Oct. 2022.

[7] E. Gandini et al., "A dielectric dome antenna with reduced profile and wide scanning capability," *IEEE Trans. Antennas Propag.*, vol. 69, no. 2, pp. 747–759, Feb. 2021.

[8] Y. Youn et al., "Dome-shaped mmWave lens antenna optimization for wide-angle scanning and scan loss mitigation using geometric optics and multiple scattering," *IEEE J. Multiscale Multiphys. Comput. Techn.*, vol. 7, pp. 142–150, 2022.

[9] P. S. Hall and S. J. Vetterlein, "Review of radio frequency beamforming techniques for scanned and multiple beam antennas," *IEE Proc. H (Microw., Antennas Propag.)*, vol. 137, pp. 293–303, Oct. 1990.

[10] P. Angeletti and M. Lisi, "Beam-forming network developments for European satellite antennas," *Microw. J.*, vol. 50, p. 58, Aug. 2007.

[11] P. Angeletti and M. Lisi, "Multimode beamforming networks for space applications," *IEEE Antennas Propag. Mag.*, vol. 56, no. 1, pp. 62–78, Feb. 2014.

[12] Y. J. Guo, M. Ansari, and N. J. G. Fonseca, "Circuit type multiple beamforming networks for antenna arrays in 5G and 6G terrestrial and non-terrestrial networks," *IEEE J. Microw.*, vol. 1, no. 3, pp. 704–722, Jul. 2021.

[13] F. Pizarro, D. Ramírez-Gil, A. Algaba-Brazález, L. F. Herrán-Ontanón, and E. Rajo-Iglesias, "Comparison study of 4×4 butler matrices in microstrip technologies for Ka-band," *AEU-Int. J. Electron. Commun.*, vol. 122, Jul. 2020, Art. no. 153248.

[14] W. Rotman, "Wide-angle scanning with microwave double-layer pillboxes," *IRE Trans. Antennas Propag.*, vol. 6, no. 1, pp. 96–105, Jan. 1958.

[15] V. Mazzola and J. E. Becker, "Coupler-type bend for pillbox antennas," *IEEE Trans. Microw. Theory Techn.*, vol. 15, no. 8, pp. 462–468, Aug. 1967.

[16] M. Ettorre, R. Sauleau, and L. Le Coq, "Multi-beam multi-layer leaky-wave SIW pillbox antenna for millimeter-wave applications," *IEEE Trans. Antennas Propag.*, vol. 59, no. 4, pp. 1093–1100, Apr. 2011.

[17] W. Rotman and R. Turner, "Wide-angle microwave lens for line source applications," *IEEE Trans. Antennas Propag.*, vol. 11, no. 6, pp. 623–632, Nov. 1963.

[18] Y. J. Cheng et al., "Substrate integrated waveguide (SIW) Rotman lens and its Ka-band multibeam array antenna applications," *IEEE Trans. Antennas Propag.*, vol. 56, no. 8, pp. 2504–2513, Aug. 2008.

[19] N. J. G. Fonseca, "A focal curve design method for Rotman lenses with wider angular scanning range," *IEEE Antennas Wireless Propag. Lett.*, vol. 16, pp. 54–57, 2017.

[20] O. Quevedo-Teruel, J. Miao, M. Mattsson, A. Algaba-Brazalez, M. Johansson, and L. Manholm, "Glide-symmetric fully metallic Luneburg lens for 5G communications at Ka-band," *IEEE Antennas Wireless Propag. Lett.*, vol. 17, pp. 1588–1592, 2018.

[21] O. Quevedo-Teruel et al., "Geodesic lens antennas for 5G and beyond," *IEEE Commun. Mag.*, vol. 60, no. 1, pp. 40–45, Jan. 2022.

[22] T. Ströber, S. Tubau, E. Girard, H. Legay, G. Goussetis, and M. Ettorre, "Shaped parallel-plate lens for mechanical wide-angle beam steering," *IEEE Trans. Antennas Propag.*, vol. 69, no. 12, pp. 8158–8169, Dec. 2021.

[23] D. F. Filipovic, S. S. Gearhart, and G. M. Rebeiz, "Double-slot antennas on extended hemispherical and elliptical silicon dielectric lenses," *IEEE Trans. Microw. Theory Techn.*, vol. 41, no. 10, pp. 1738–1749, Oct. 1993.

[24] C. A. Fernandes, "Shaped dielectric lenses for wireless millimeter-wave communications," *IEEE Antennas Propag. Mag.*, vol. 41, no. 5, pp. 141–150, Oct. 1999.

[25] G. Godi, R. Sauleau, and D. Thouroude, "Performance of reduced size substrate lens antennas for millimeter-wave communications," *IEEE Trans. Antennas Propag.*, vol. 53, no. 4, pp. 1278–1286, Apr. 2005.

[26] H. Kawahara, H. Deguchi, M. Tsuji, and H. Shigesawa, "Design of rotational dielectric dome with linear array feed for wide-angle multibeam antenna applications," *Electron. Commun. Jpn. (Part II, Electron.)*, vol. 90, pp. 49–57, May 2007.

[27] C. A. Fernandes, E. B. Lima, and J. R. Costa, "Dielectric lens antennas," in *Handbook of Antenna Technologies*, Z. Chen Eds. Singapore, Springer, 2015.

[28] J. R. Costa, M. G. Silveirinha, and C. A. Fernandes, "Evaluation of a double-shell integrated scanning lens antenna," *IEEE Antennas Wireless Propag. Lett.*, vol. 7, pp. 781–784, 2008.

[29] J. R. Costa, C. A. Fernandes, G. Godi, R. Sauleau, L. Le Coq, and H. Legay, "Compact Ka-band lens antennas for LEO satellites," *IEEE Trans. Antennas Propag.*, vol. 56, no. 5, pp. 1251–1258, May 2008.

[30] J. R. Costa, E. B. Lima, and C. A. Fernandes, "Compact beam-steerable lens antenna for 60-GHz wireless communications," *IEEE Trans. Antennas Propag.*, vol. 57, no. 10, pp. 2926–2933, Oct. 2009.

[31] J. Budhu and Y. Rahmat-Samii, "A novel and systematic approach to inhomogeneous dielectric lens design based on curved ray geometrical optics and particle swarm optimization," *IEEE Trans. Antennas Propag.*, vol. 67, no. 6, pp. 3657–3669, Jun. 2019.

[32] L. Xiao, S.-W. Qu, and S. Yang, "3-D printed dielectric dome array antenna with ±80° beam steering coverage," *IEEE Trans. Antennas Propag.*, vol. 70, no. 11, pp. 10494–10503, Nov. 2022.

[33] A. Algaba-Brazalez, P. Castillo-Tapia, M. C. Vigano, and O. Quevedo-Teruel, "Lenses combined with array antennas for the next generation of terrestrial and satellite communication systems," *IEEE Commun. Mag.*, early access, Oct. 9, 2023, doi: 10.1109/MCOM.024.2300370.

[34] A. Algaba-Brazález, H. Wang, P. Castillo-Tapia, L. Manholm, M. Johansson, and O. Quevedo-Teruel, "Flexible 6G antenna systems based on innovative lenses combined with array antennas," in *Proc. 17th Eur. Conf. Antennas Propagat. (EuCAP)*, 2023, pp. 1–5.

[35] H. Wang, P. Castillo-Tapia, L. Manholm, M. Johansson, O. Quevedo-Teruel, and A. Algaba-Brazález, "6G energy-efficient systems based on arrays combined with dielectric lenses," *Electron. Lett.*, vol. 59, no. 17, 2023, Art. no. e12932.

[36] H. Steyskal, A. Hessel, and J. Shmoys, "On the gain-versus-scan trade-offs and the phase gradient synthesis for a cylindrical dome antenna," *IEEE Trans. Antennas Propag.*, vol. 27, no. 6, pp. 825–831, Nov. 1979.

[37] A. Benini et al., "Phase-gradient meta-dome for increasing grating-lobe-free scan range in phased arrays," *IEEE Trans. Antennas Propag.*, vol. 66, no. 8, pp. 3973–3982, Aug. 2018.

[38] D. C. Mu and R. Rudduck, "Plane wave spectrum-surface integration technique for radome analysis," *IEEE Trans. Antennas Propag.*, vol. 22, no. 3, pp. 497–500, May 1974.

[39] P. Einziger and L. Felsen, "Ray analysis of two-dimensional radomes," *IEEE Trans. Antennas Propag.*, vol. 31, no. 6, pp. 870–884, Nov. 1983.

[40] N. N. Youssef, "Radar cross section of complex targets," *Proc. IEEE*, vol. 77, no. 5, pp. 722–734, May 1989.

[41] M. Domingo, F. Rivas, J. Perez, R. P. Torres, and M. F. Catedra, "Computation of the RCS of complex bodies modeled using NURBS surfaces," *IEEE Antennas Propag. Mag.*, vol. 37, no. 6, pp. 36–47, Dec. 1995.

[42] F. S. de Adana, I. G. Diego, O. G. Blanco, P. Lozano, and M. F. Catedra, "Method based on physical optics for the computation of the radar cross section including diffraction and double effects of metallic and absorbing bodies modeled with parametric surfaces," *IEEE Trans. Antennas Propag.*, vol. 52, no. 12, pp. 3295–3303, Dec. 2004.

[43] F. Weinmann, "Ray tracing with PO/PTD for RCS modeling of large complex objects," *IEEE Trans. Antennas Propag.*, vol. 54, no. 6, pp. 1797–1806, Jun. 2006.

[44] V. I. Litun and V. N. Mitrokhin, "Waveguide-based dome lens antenna with quasioptimal shape generating line," in *Proc. IEEE Int. Conf. Microw. Technol. Comput. Electrom.*, 2013, pp. 296–299.

[45] W.-J. Zhao, Y.-B. Gan, L.-W. Li, and C.-F. Wang, "Effects of an electrically large airborne radome on radiation patterns and input impedance of a dipole array," *IEEE Trans. Antennas Propag.*, vol. 55, no. 8, pp. 2399–2402, Aug. 2007.

[46] C. D. Giovampaola, G. Carluccio, F. Puggelli, A. Toccafondi, and M. Albani, "Efficient algorithm for the evaluation of the physical optics scattering by NURBS surfaces with relatively general boundary condition," *IEEE Trans. Antennas Propag.*, vol. 61, no. 8, pp. 4194–4203, Aug. 2013.

[47] Z. Asadi and V. Mohtashami, "Efficient meshing scheme for bodies of revolution-application to physical optics prediction of electromagnetic scattering," *Prog. Electromagn. Res. M*, vol. 48, pp. 163–172, Jan. 2016.

[48] E. Garcia, C. Delgado, and M. F. Catedra, "A novel and efficient technique based on the characteristic basis functions method for solving scattering problems," *IEEE Trans. Antennas Propag.*, vol. 67, no. 5, pp. 3241–3248, May 2019.

[49] A. Paraskevopoulos, F. Maggiorelli, M. Albani, and S. Maci, "Radial GRIN lenses based on the solution of a regularized ray congruence equation," *IEEE Trans. Antennas Propag.*, vol. 70, no. 2, pp. 888–899, Feb. 2022.

[50] X. Sheng, Y. Zhang, R. Shen, and N. Liu, "A cylindrical equivalent source-based physical optics method for rapid analysis of airborne radomes," *IEEE Access*, vol. 10, pp. 99282–99289, 2022.

[51] H. Ke, P. Wang, J. Liu, J. Li, and M. He, "A hybrid method for fast and efficient evaluation of electromagnetic performance of the radome-enclosed antennas," *IEEE Trans. Antennas Propag.*, vol. 70, no. 10, pp. 9795–9805, Oct. 2022.

[52] "Ticra GRASP." Ticra.com. 2022, Accessed: Jun. 2023. [Online]. Available: https://www.ticra.com/software/grasp/

[53] (Altair Eng. Inc, Troy, MI, USA). *Altair Feko, NewFASANT*. Accessed: Jun. 2023. [Online]. Available: https://www.altair.com/feko

[54] Q. Liao, N. J. G. Fonseca, M. Camacho, Á. Palomares-Caballero, F. Mesa, and O. Quevedo-Teruel, "Ray-tracing model for generalized geodesic multiple beam lens antennas," *IEEE Trans. Antennas Propag.*, vol. 71, no. 3, pp. 2640–2651, Mar. 2023.

[55] E. Lima, J. R. Costa, M. G. Silreirinha, and C. A. Fernandes, "ILASH–software tool for the design of integrated lens antennas," in *Proc. IEEE Antennas Propag. Soc. Int. Symp.*, 2008, pp. 1–4.

[56] M. J. Hayford. "Ray-optics." Accessed: Jun. 2023. [Online]. Available: https://github.com/mjhoptics/ray-optics

[57] "pyoptools." 2022, Accessed: Jun. 2023. [Online]. Available: https://github.com/cihologramas/pyoptools

[58] M. Born and E. Wolf, *Principles of Optics: Electromagnetic Theory of Propagation, Interference, and Diffraction of Light*, 6th ed., Oxford, U.K.: Pergamon Press, 1964.

[59] J. D. Joannopoulos, S. G. Johnson, J. N. Winn, and R. D. Meade, *Photonic Crystals: Molding the Flow of Light*, 2nd ed., Princeton, NJ, USA: Princeton Univ. Press, 2007.

[60] W. C. Chew, *Waves and Fields in Inhomogeneous Media*, D. G. Dudley, ed., Piscataway, NJ, USA: IEEE Press, 1995.

[61] D. Kozakoff, *Analysis of Radome Enclosed Antennas*, 2nd ed., Morristown, NJ, USA: Artech, 2009.

[62] M. Sebastian, M. Silva, and A. Sombra, *Measurement of Microwave Dielectric Properties and Factors Affecting Them*. Hoboken, NJ, USA: Wiley, 2017, pp. 1–51.

[63] R. E. Collin, *Field Theory of Guided Waves*, 2nd ed., Piscataway, NJ, USA: IEEE-Press, 1991.

[64] S. Orfanidis, *Electromagnetic Waves and Antennas*, Rutgers Univ., Piscataway, NJ, USA, 2016.

MARIA PUBILL-FONT received the bachelor's degree in telecommunications engineering from Ramon Llull University, Barcelona, Spain, in 2016, and the double master's degree in telecommunications engineering from the Polytechnic University of Catalonia, Barcelona, Spain, and the Royal Institute of Technology, Stockholm, Sweden, in 2023. She is currently pursuing the Ph.D. degree in millimeter and submillimeter band antennas with the University of Technology Sydney, Sydney, Australia. Her current research interests include lens antennas, transformation optics, antenna array technologies, and beamforming networks.

FRANCISCO MESA (Fellow, IEEE) received the Licenciado and Ph.D. degrees in physics from the Universidad de Sevilla, Seville, Spain, in 1989 and 1991, respectively, where he is currently a Professor with the Departamento de Física Aplicada 1. His research interest includes electromagnetic propagation/radiation in microwave and quasi-optical structures.

ASTRID ALGABA-BRAZÁLEZ received the degree in telecommunication engineering from the Miguel Hernández University of Elche, Alicante, Spain, in 2009, and the Licentiate of Engineering and Ph.D. degrees from the Chalmers University of Technology, Gothenburg, Sweden, in 2013 and 2015, respectively.

She joined the Ericsson Research Department, Gothenburg, in November 2014, where she currently works as a Master Researcher and a Project Manager of the Program "Hardware Research for Array Antenna integration at mm-wave frequencies." Her work is focused on 5G/6G Antenna hardware projects (including contributing to coordinate, design, implement and evaluate active antenna system testbed demonstrators for future communication systems). She has also been leading all research activities related to metasurfaces and lens antennas within Ericsson Research since 2015. Her research interests include millimeter-wave and sub-THz antenna technologies for 5G/6G radio access applications, lens antennas, leaky wave antennas, radomes, design of microwave passive components, metasurfaces, system integration of active components and antennas, and investigation of routing methods to achieve such integration. Moreover, she received the second Best Paper Award at the International Symposium on Antennas and Propagation held in 2017 and the Best Paper Award in Antennas at the European Conference on Antennas and Propagation held in 2020. She is also co-recipient of the Best Student Paper Award and the Student Honorable Mention at ISAP2022. She is one of the two Swedish Delegates and management committee member of the European COST Action SYMAT- CA18223- Future communications with higher-symmetric engineered artificial materials, and currently serves as an Associate Editor for IEEE ANTENNAS AND WIRELESS PROPAGATION LETTERS.

SARAH CLENDINNING was born in Lurgan, Northern Ireland, in 1995. She received the M.Sci. degree in physics and the Ph.D. degree from Queen's University Belfast, Northern Ireland, in 2017 and 2021, respectively. Since 2021, she has been a Postdoctoral Researcher with the KTH Royal Institute of Technology, Stockholm, Sweden. Her current research interests lie in geodesic lens antennas, Luneburg lens antennas, periodic structures and ray-tracing techniques in geodesic lenses and radomes. She was a recipient of the Best Student Paper Award at the Loughborough Antennas and Propagation Conference in 2018 and the Best Young Professional Paper Award at the International Symposium on Antennas and Propagation in 2022.

MARTIN JOHANSSON (Senior Member, IEEE) received the M.Sc. degree in engineering physics and the Ph.D. degree in electromagnetics from the Chalmers University of Technology in 1986 and 1997, respectively.

He joined Ericsson Research, Ericsson AB, Gothenburg, Sweden, in 1997, where he currently serves as an Expert of Antenna Technology. His current research interests include antenna technology for mobile communications, antenna system modeling, and deterministic channel modeling.

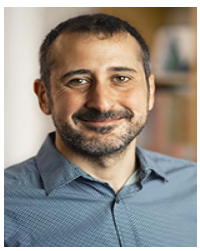

OSCAR QUEVEDO-TERUEL (Fellow, IEEE) received the degree in telecommunication engineering and the Ph.D. degree from the Carlos III University of Madrid, Spain, in 2005 and 2010, respectively. From 2010 to 2011, he joined the Department of Theoretical Physics of Condensed Matter, Universidad Autonoma de Madrid as a Research Fellow and went on to continue his postdoctoral research with the Queen Mary University of London from 2011 to 2013. In 2014, he joined the Division of Electromagnetic Engineering and Fusion Science, School of Electrical Engineering and Computer Science, KTH Royal Institute of Technology in Stockholm, Sweden, where he is a Professor and the Director of the Master Programme in Electromagnetics Fusion and Space Engineering. He is the coauthor of more than 140 papers in international journals and more than 240 at international conferences. He was an Associate Editor of the IEEE TRANSACTIONS ON ANTENNAS AND PROPAGATION from 2018 to 2022, and has been acting as a Track Editor in IEEE TAP since 2022. He was a Distinguished Lecturer of the IEEE Antennas and Propagation Society from 2019 to 2022. He has been a member of the European Association on Antennas and Propagation (EurAAP) Board of Directors since January 2021. Since January 2022, he has been the Vice-Chair of EurAAP. He has made scientific contributions to higher symmetries, transformation optics, lens antennas, metasurfaces, and high impedance surfaces.